mathematics

MDPI

Article

Nonlinear Analysis of the Multi-Layered Nanoplates

Mostafa Sadeghian *, Arvydas Palevicius, Paulius Griskevicius and Giedrius Janusas *

Faculty of Mechanical Engineering and Design, Kaunas University of Technology, Studentu 56, 51424 Kaunas, Lithuania

* Correspondence: mostafa.sadeghian@ktu.edu (M.S.); giedrius.janusas@ktu.lt (G.J.)

Abstract: This text investigates the bending/buckling behavior of multi-layer asymmetric/symmetric annular and circular graphene plates through the application of the nonlocal strain gradient model. Additionally, the static analysis of multi-sector nanoplates is addressed. By considering the van der Waals interactions among the layers, the higher-order shear deformation theory (HSDT), and the nonlocal strain gradient theory, the equilibrium equations are formulated in terms of generalized displacements and rotations. The mathematical nonlinear equations are solved utilizing either the semi-analytical polynomial method (SAPM) and the differential quadrature method (DQM). Also, the available references are used to validate the results. Investigations are conducted to examine the effect of small-scale factors, the van der Waals interaction value among the layers, boundary conditions, and geometric factors.

Keywords: nonlinear analysis; nonlocal strain gradient theory; multi-layered nanoplates; DQM; SAPM

MSC: 35Q74; 65N22

1. Introduction

A new era in science can be attributed to the development of nanotechnology. Many researchers have become interested in nanostructures since the discovery of carbon nanotubes. Initial research revealed that nanostructures' mechanical characteristics differ from those of other materials. Because of these unique qualities, nanostructures are now employed in a wide range of applications, such as electric batteries, nanocomposites, nanoactuators, nanosensors, and nanobearings [1–3]. Graphene sheets, which are formed by forming carbon nanotubes, are one type of nanostructure. Other types of nanostructures include nanowires, nanorings, and nanorods [4]. With its hexagonal crystal lattice structure and thickness equivalent to that of a carbon atom, graphene exhibits exceptional mechanical and physical characteristics such as high tensile strength, high flexibility, and high thermal and electrical conductivity, among others [5].

There are two methods for modeling nanostructures: continuum mechanics and molecular dynamics (MD) simulation. When dealing with many atoms, the MD method requires a substantial amount of computational effort. Studies conducted through experimentation have demonstrated that structures' mechanical properties at very small scales can differ from those at macroscales. Because classical continuum mechanics models are unable to take small-scale effects into account, they cannot predict the properties of nanostructures. Various models of nonclassical continuum mechanics have been developed to surmount these challenges, such as strain gradient theory, couple stress theory, and nonlocal elasticity theory. These models were developed to overcome the limitations of traditional approaches and offer a more complete understanding of the mechanical properties of nanoscale structures [6].

Eringen [7] added non-local effects to classical elasticity theory by introducing a nonlocal elasticity model. In this theory, the entire material domain influences the stress at a given location. Yang and his colleagues [8] created a couple stress theory by taking strain

check for updates

Citation: Sadeghian, M.; Palevicius, A.; Griskevicius, P.; Janusas, G. Nonlinear Analysis of the Multi-Layered Nanoplates. *Mathematics* **2024**, *12*, 3545. https://doi.org/10.3390/math12223545

Academic Editor: Alicia Cordero

Received: 17 October 2024
Revised: 5 November 2024
Accepted: 6 November 2024
Published: 13 November 2024

gradients from symmetry rotation into account. Moreover, the modified strain gradient theory was developed by Lam et al. [9] to investigate the effects of strain gradients, such as deviatoric stretch gradient, symmetry rotation gradient, and dilatation gradient. These theoretical frameworks consider the influence of strain gradients or nonlocal factors.

Only nanostructures with softening behavior can be modeled by nonlocal elastic models, suggesting that "smaller is more compliant" [10]. According to the gradient elasticity theory, extra strain gradient terms should be included in the total stress and nanostructures can be represented as atoms with higher-order mechanical properties instead of as collections of points [11]. However, this theory does not take into account the inter-atomic long-range force. Moreover, gradient elasticity theory, which suggests that "smaller is stiffer", can only simulate hardening nanostructures [10]. Therefore, it is necessary to integrate both theories in order to model nanostructures that exhibit both hardening and softening behavior. Tian et al. [12] reported experimental evidence of this kind of response. The nonlocal strain gradient theory was created by Lim and his associates [13], which essentially combines the nonlocal and strain gradient theories into a single theory by requiring that the stress tensor take into consideration the contributions of both the nonlocal stress tensor and the strain gradient stress tensor. This theory takes into account the nonlocal effects of strain gradients within the material, meaning that it takes into account how nearby material points affect the deformation behavior. The nonlocal strain gradient and length scale are important parameters in this theory. It is the characteristic length over which the deformation of adjacent material points is influenced by the nonlocal length scale. Variations in strain within the material are taken into account by the strain gradient. To capture the size-dependent mechanical behavior of materials, especially at the nanoscale, nonlocal strain gradient theory is used [14].

Several studies on the size-dependent characteristics of nanostructures have been conducted [15–19]. Using nonlocal strain gradient theory, research was performed by Gui and Wu [20] on the buckling of a thermal- electric-elastic nano cylindrical shell under axial load. Also, they found that the strain gradient parameter had less of an impact on the buckling load of nano cylindrical shells than the nonlocal coefficient. A size-dependent classical model was proposed by Lu and his colleagues [21] to examine the buckling of rectangular nanoplates. Arefi et al. [22] presented the bending examination of sandwich plates with porosity using FSDT and the nonlocal strain gradient theory. Using a higher-order nonlocal strain gradient theory, Farajpour et al. [23] examined the buckling of orthotropic nanoplates in the thermal environment. They discovered that the buckling load is almost completely affected by the nonlocal parameter. A similar approach was used in ref. [24] to investigate the nonlinear vibration of sandwich nanoplates, and it was found that small-scale parameter influence on the nonlinear frequency increased with vibration amplitude. Thai et al. [25] used nonlocal strain gradient theorem to examine the vibrations of FG annular nanoplates composed of magnetic- elastic-electrical properties. The natural frequencies derived from circular nanoplates were demonstrated to be higher than those anticipated with annular ones. Also, Thai and colleagues [26] conducted a study on the free vibration analysis of functionally graded (FG) rectangular nanoplates using the nonlocal strain gradient theory and higher-order shear deformation theorem. Alghanmi [27] studied the bending of porous plates via the nonlocal strain gradient theory and noticed that plates with even porosities deflect more than those with uneven porosities. Siddique and Nazmul [28] carried out the bending examination of functionally graded beams with the aid of the nonlocal strain gradient theorem and nonlocal couple stress model via the Laplace transform method. By applying the Galerkin method to the first-order shear deformation theory, the nonlinear static examination of hygrothermal magneto-electro-elastic nanoplates while taking the flexo-magneto-electric effect into account was investigated in ref. [18]. Phung-Van et al. [29] analyzed the small-scale examination of FG nanoplates with the triply periodic minimal surface property. The study shows how adjusting the nonlocal and strain gradient parameters can help understand the mechanisms that both increase and decrease stiffness in the nanoplate. Thai and his colleagues [25] investigated the free vibrations of FG nanoplates

with magnetic, electric and elastic properties using the nonlocal strain gradient theorem and the higher-order shear deformation theory. Through the manipulation of two parameters, their method captures the nonlocal and strain gradient effects in nanoplates, which lead to increased stiffness and decreased stiffness, respectively. Liu et al. [30] examined the bending of thin rectangular plates. Gao et al. [31] studied the nonlinear bending of a cantilever beam subjected to different types of loading. Also, Wang and his colleague [32] performed the bending investigation of rectangular nanolaminates with the aid of the Kirchhoff model. They showed that surface effects diminish the values of the deflection. Moreover, Krysko et al. [33] analyzed the static investigation of nanoplates exposed to distributed loads and local areas via the modified couple stress model. They showed that the stress–strain state is reduced (deflection and stress) for various environments and types of loads by enhancing the size–dependent parameter.

Also, recently, many papers have studied nonlinear analyses and using different numerical techniques [34–36]. For example, Wu and his colleagues [37] studied the nonlinear static examination of nanobeams with longitudinal linear temperature gradients based on nonlocal stress gradient theory via the Galerkin method. Using DQM, Shan et al. [38] investigated the nonlinear vibration of the FGM piezoelectric micro/nanobeam incorporating flexoelectric effect based on the Euler beams model and the extended dielectric theorem. Using the fourth-order Runge–Kutta method and Airy stress functions as well as the Galerkin technique, Cong and Duc [36] studied the nonlinear static and dynamic of nanoplate with the graphene platelet–reinforcement nonlocal elasticity theorem and classical plate model. Using the finite element method, Phuc et al. [39] analyzed the free vibration and the bending of composite nanoplates based on the nonlocal theory and third-order shear deformation model.

The literature states that, mainly, studies have been conducted to examine how nano beams/plates behave in Cartesian coordinates and using first-order shear deformation theory. Nevertheless, there are fewer studies of nanoplates in polar coordinates (circular/annular/sector plates) than there are of beams or rectangular graphene sheets. Until now, there has been no work considering multilayer graphene plates using nonlocal strain gradient theory as well as HSDT considering polar coordinates. This paper employs the nonlocal strain gradient theory as well as HSDT to examine the bending/buckling of circular/annular multilayer nanoplates considering the nonlocal strain gradient theorem. Also, the static study of multi-sector nanoplates is addressed. Moreover, geometry, values of the elastic foundation, small-scale parameters, and various boundary conditions are examined. This investigation offers a theoretical foundation that can contribute to the design and advancements of nanodevices.

2. The Governing Equations

Multiple layers of graphene can be employed to overcome the limited bending strengths of graphene sheets. Layers of graphene are thus created by stacking graphene sheets on top of one another and joining them using van der Waals force [40]. The Lennard–Jones potential model is used to simulate the van der Waals interaction forces between the layers as a set of springs [41,42]. Figure 1 depicts a multi-layer graphene sheet under uniform transverse loading q, with thickness h. Also, k_0 is defined as the van der Waals stiffness coefficient among layers. Furthermore, k_w and k_p are defined as the coefficients of the Winkler as well as Pasternak elastic foundations. Moreover, Figure 2. displays the bottom layer of the graphene annular plate on elastic foundations with inner radius r_i, and outer radius r_o. The displacement field (considering the HSDT) can be expressed as follows:

$$\begin{array}{l} U_i(r,\theta,z) = u_i(r) - z\frac{dw_i(r)}{dr} + g(z)\phi_i(r) \\ V_i(r,\theta,z) = 0 \\ W_i(r,\theta,z) = w_i(r)\ , i = 1,\ldots n \end{array} \quad (1)$$

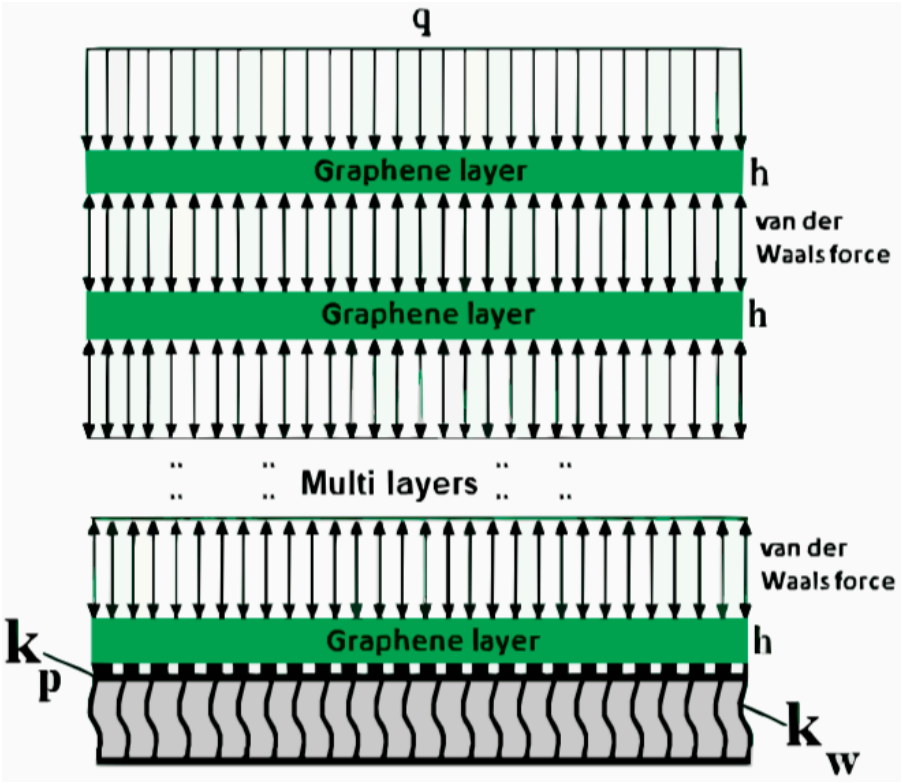

Figure 1. The multi-layer graphene annular plate under bending loads.

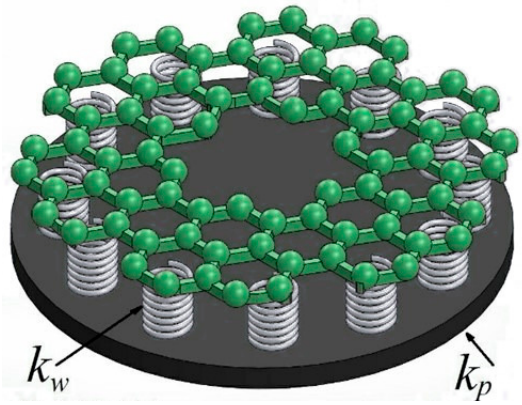

Figure 2. The bottom layer of the graphene annular plate on the Pasternak-Winkler elastic foundation.

It should be noted that in the above equations, the layer number is represented by the index i; for instance, $i = 1$ denotes the upper layer that is subject to a transverse load, and $i = n$ denotes the lower layer that is supported by an elastic foundation ($i = 1, 2, \ldots n$).

u_0, v_0, and w_0 can be defined as the displacement components of the midplane in the r, θ, and z directions, respectively. Also, ϕ is the rotation component in the θ axis. The function $g(z)$ is defined as follows.

$$g(z) = f(z) + zy^* \tag{2}$$

$f(z)$ and y^* are different functions that have been utilized in different references and can be seen in Table 1.

Table 1. The $g(z)$ functions considered by different authors.

Model	$g(z)$ **Function**
Ambartsumian [40]	$-\frac{1}{6}z^3+\frac{h^2}{8}z$
Reddy [43]	$-\frac{4}{3h^2}z^3+z$
Reissner [44]	$-\frac{5}{3h^2}z^3+\frac{5}{4}z$
Touratier [45]	$\frac{h}{\pi}\sin\left(\frac{\pi z}{h}\right)$
Soldatos [46]	$h\sinh\left(\frac{z}{h}\right)-z\cosh\left(\frac{1}{2}\right)$
Aydogdu [47]	$ze^{-2\left(\frac{z}{h}\right)^2}$
Mantari [48]	$\frac{h}{\pi}\left(\sin\left(\frac{\pi z}{h}\right)e^{m\cos\left(\frac{\pi z}{h}\right)}+m\frac{\pi}{h}z\right)$, $m\geq 0$

Based on the von Karman presumptions, strain components are as follows:

$$\varepsilon_{ir}=\frac{dU_i}{dr}+\frac{1}{2}\left(\frac{dW_i}{dr}\right)^2=\frac{du_i}{dr}-z\frac{d^2w_i}{dr^2}+g(z)\frac{d\phi_i}{dr}+\frac{1}{2}\left(\frac{dw_i}{dr}\right)^2 \tag{3}$$

$$\varepsilon_{i\theta}=\frac{U_i}{r}=\frac{1}{r}\left(u_i-z\frac{dw_i}{dr}+g(z)\phi_i\right) \tag{4}$$

$$\gamma_{ir\theta}=0 \tag{5}$$

$$\gamma_{irz}=\frac{dW_i}{dr}+\frac{dU_i}{dz}=\phi_i\frac{dg(z)}{dz} \tag{6}$$

$$\gamma_{i\theta z}=0 \tag{7}$$

Lim et al. [13] developed the nonlocal strain gradient theory which can be expressed as follows:

$$(1-\mu^2\nabla^2)\sigma_{ij}=C_{ijkl}(1-l^2\nabla^2)\varepsilon_{kl},\ \nabla^2=\frac{d^2}{dr^2}+\frac{1}{r}\frac{d}{dr} \tag{8}$$

In Equation (8) the nonlocal, strain gradient and elastic coefficients are μ, l, and C_{ijkl}, respectively. Also, the constitutive mathematical relationship for stress–strain at the nanoscale can be seen in Equation (9) [49]:

$$\begin{gathered}(1-\mu^2\nabla^2)\begin{bmatrix}\sigma_r\\ \sigma_\theta\\ \sigma_{rz}\end{bmatrix}=(1-l^2\nabla^2)\begin{bmatrix}Q_{11}&Q_{12}&0\\ Q_{12}&Q_{22}&0\\ 0&0&G_{13}\end{bmatrix}\begin{bmatrix}\varepsilon_r\\ \varepsilon_\theta\\ \gamma_{rz}\end{bmatrix},\\ Q_{11}=\frac{E_1}{1-\nu_{12}\nu_{21}},Q_{22}=\frac{E_2}{1-\nu_{12}\nu_{21}},\ Q_{12}=\frac{\nu_{12}E_2}{1-\nu_{12}\nu_{21}},G_{13}=\frac{E_1}{2(1+\upsilon_{12})}\end{gathered} \tag{9}$$

It is noted that in Equation (9), E_1 and E_2 are the Young's modulus along 1 and 2 directions. Also v_{12} and v_{21} are Poisson's ratios. G_{12}, G_{13} and G_{23} can be written as the shear moduli.

Considering the nonlocal form (NL), the force as well as momentum resultants can be written as given below:

$$\{N_{ir},N_{i\theta},Q_{ir}\}^{NL}=\int_{-\frac{h}{2}}^{\frac{h}{2}}\{\sigma_{ir},\sigma_{i\theta},\sigma_{irz}\}^{NL}dz \tag{10}$$

$$\{M_{ir},M_{i\theta}\}^{NL}=\int_{-\frac{h}{2}}^{\frac{h}{2}}\{\sigma_{ir},\sigma_{i\theta}\}^{NL}zdz \tag{11}$$

$$\{R_{ir},R_{i\theta}\}^{NL}=\int_{-\frac{h}{2}}^{\frac{h}{2}}\{\sigma_{ir},\sigma_{i\theta}\}^{NL}f(z)dz \tag{12}$$

$$R_{irz}^{NL} = \int_{-\frac{h}{2}}^{\frac{h}{2}} \sigma_{irz}^{NL} f'(z) dz \tag{13}$$

The system's potential energy is described as follows [50]:

$$\Pi = U_i + \Omega_i \tag{14}$$

U can be defined as the strain energy, Π is the potential energy, and Ω can be defined as the potential energy of external forces. Also, taking into account the principle of minimum potential energy, the variation in the potential energy of the system in the equilibrium state is equal to zero [50]:

$$\delta\Pi = \delta U_i + \delta\Omega_i = 0 \tag{15}$$

Therefore,

$$\delta U = \iiint_V (\sigma_{ir}\delta\varepsilon_{ir} + \sigma_{i\theta}\delta\varepsilon_{i\theta} + \sigma_{irz}\delta\gamma_{irz}) dV \tag{16}$$

Moreover,

$$\delta\Omega_1 = \int_{r_i}^{r_o} \int_0^{2\pi} (q + k_o(w_2 - w_1))\delta w r dr d\theta : \text{ Upper layer} \tag{17}$$

$$\delta\Omega_i = \int_{r_i}^{r_o} \int_0^{2\pi} (-k_o(w_i - w_{i-1}) + k_o(w_{i+1} - w_i))\delta w r dr d\theta, \ (\mathrm{i} = 2 \ldots, \mathrm{n} - 1) \tag{18}$$

$$\delta\Omega_n = \int_{r_i}^{r_o} \int_0^{2\pi} \left(-k_o(w_n - w_{n-1}) - k_w w_n + k_p \nabla^2 w_n\right)\delta w r dr d\theta : \text{Bottom layer} \tag{19}$$

In Equation (19), k_w and k_p depict the Winkler as well as Pasternak elastic foundation coefficients, respectively. By setting $\delta\Pi$ to zero, the coefficients of $\delta u, \delta w$, and $\delta\phi$ are considered equal to zero, and the Euler–Lagrange mathematical relations can be written as follows:

$$\delta u_i : N i_r^{NL} + r\frac{dN i_r^{NL}}{dr} - N i_\theta^{NL} = 0 \, , i = 1, \ldots n \tag{20}$$

$$\begin{aligned} \delta w_1 : r\tfrac{d^2 M_{1r}^{NL}}{dr^2} + 2\tfrac{dM_{1r}^{NL}}{dr} - \tfrac{dM_{1\theta}^{NL}}{dr} + ((q + k_0(w_2 - w_1))r + \\ N_{1\theta}^{NL}\tfrac{dw_1}{dr} + r N_{1r}^{NL}\tfrac{d^2 w_1}{dr^2}\Big) = 0 \end{aligned} \tag{21}$$

$$\begin{aligned} \delta w_i : r\tfrac{d^2 M_{ir}^{NL}}{dr^2} + 2\tfrac{dM_{ir}^{NL}}{dr} - \tfrac{dM_{i\theta}^{NL}}{dr} + ((-k_0(w_i - w_{i-1}) + k_0(w_i - w_{i-1}))r + \\ N_{i\theta}^{NL}\tfrac{dw_i}{dr} + r N_{ir}^{NL}\tfrac{d^2 w_i}{dr^2}\Big) = 0, \ (i = n - 1) \end{aligned} \tag{22}$$

$$\begin{aligned} \delta w_n : r\tfrac{d^2 M_{nr}^{NL}}{dr^2} + 2\tfrac{dM_{nr}^{NL}}{dr} - \tfrac{dM_{n\theta}^{NL}}{dr} + \left(\left(-k_0(w_n - w_{n-1}) - k_w w_n + k_p \nabla^2 w_n\right)r + \right. \\ \left. N_{n\theta}^{NL}\tfrac{dw_2}{dr} + r N_{nr}^{NL}\tfrac{d^2 w_n}{dr^2}\right) = 0 \end{aligned} \tag{23}$$

$$\delta\phi_i : y^*\left(r\frac{dM_{ir}^{NL}}{dr} + M_{ir}^{NL} - M_{i\theta}^{NL} - rQ_{ir}^{NL}\right) + R_{ir}^{NL} + r\frac{dR_{ir}^{NL}}{dr} - R_{i\theta}^{NL} - rR_{irz}^{NL} = 0, i = 1, \ldots n \tag{24}$$

It is noted that the nonlocal form can be considered as follows:

$$\left(1 - \mu\nabla^2\right)\{N_{ir}, N_{i\theta}, Q_{ir}\}^{NL} = \int_{-\frac{h}{2}}^{\frac{h}{2}} \left(1 - \mu\nabla^2\right)\{\sigma_{ir}, \sigma_{i\theta}, \sigma_{irz}\}^{NL} dz \tag{25}$$

The following are the local form resultants for force and moment:

$$\{N_{ir}, N_{i\theta}, Q_{ir}\}^L = \int_{-\frac{h}{2}}^{\frac{h}{2}} \{\sigma_{ir}, \sigma_{i\theta}, \sigma_{irz}\}^L dz \tag{26}$$

$$\{M_{ir}, M_{i\theta}\}^L = \int_{-\frac{h}{2}}^{\frac{h}{2}} \{\sigma_{ir}, \sigma_{i\theta}\}^L z dz \tag{27}$$

$$\{R_{ir}, R_{i\theta}\}^L = \int_{-\frac{h}{2}}^{\frac{h}{2}} \{\sigma_{ir}, \sigma_{i\theta}\}^L f(z) dz \tag{28}$$

$$R_{irz}^L = \int_{-\frac{h}{2}}^{\frac{h}{2}} \sigma_{irz}^L f'(z) dz \tag{29}$$

Furthermore, the following forms of resultants are obtained with respect to displacements:

$$N_{ir}^L = (1 - l^2\nabla^2)\left\{ \frac{1}{1 - \nu_{12}\nu_{21}} (E_1 h \left(\frac{du_i}{dr} + \frac{1}{2}\left(\frac{dw_i}{dr} \right)^2 \right) + \nu_{12} E_2 h \frac{1}{r} u_i + \left(E_1 \frac{d\phi_i}{dr} + \nu_{12} E_2 \frac{1}{r} \phi_i \right) \int_{-\frac{h}{2}}^{\frac{h}{2}} f(z) dz) \right\} \tag{30}$$

$$N_{i\theta}^L = (1 - l^2\nabla^2)\left\{ \frac{1}{1 - \nu_{12}\nu_{21}} (\nu_{12} E_2 h \left(\frac{du_i}{dr} + \frac{1}{2}\left(\frac{dw_i}{dr} \right)^2 \right) + E_2 h \frac{1}{r} u_i + \left(\nu_{12} E_2 \frac{d\phi_i}{dr} + E_2 \frac{1}{r} \phi_i \right) \int_{-\frac{h}{2}}^{\frac{h}{2}} f(z) dz) \right\} \tag{31}$$

$$M_{ir}^L = (1 - l^2\nabla^2)\left\{ \frac{1}{1 - \nu_{12}\nu_{21}} (E_1 \frac{h^3}{12} \left(-\frac{d^2 w_i}{dr^2} + y^* \frac{d\phi_i}{dr} \right) + \nu_{12} E_2 \frac{h^3}{12} \left(-\frac{1}{r} \frac{dw_i}{dr} + y^* \frac{1}{r} \phi_i \right) + \left(E_1 \frac{d\phi_i}{dr} + \nu_{12} E_2 \frac{1}{r} \phi_i \right) \int_{-\frac{h}{2}}^{\frac{h}{2}} z f(z) dz) \right\} \tag{32}$$

$$M_{i\theta}^L = (1 - l^2\nabla^2)\left\{ \frac{E_2}{1 - \nu_{12}\nu_{21}} (\nu_{12} \frac{h^3}{12} \left(-\frac{d^2 w_i}{dr^2} + y^* \frac{d\phi_i}{dr} \right) + \frac{h^3}{12} \left(-\frac{1}{r} \frac{dw_i}{dr} + y^* \frac{1}{r} \phi_i \right) + \left(\nu_{12} \frac{d\phi_i}{dr} + \frac{1}{r} \phi_i \right) \int_{-\frac{h}{2}}^{\frac{h}{2}} z f(z) dz) \right\} \tag{33}$$

$$R_{ir}^{L}=(1-l^{2}\nabla^{2})\Bigg\{\frac{1}{1-\nu_{12}\nu_{21}}\Bigg(\Bigg(E_{1}\Bigg(\frac{du_{i}}{dr}+\frac{1}{2}\Big(\frac{dw_{i}}{dr}\Big)^{2}\Bigg)+\nu_{12}E_{2}\frac{1}{r}u_{i}\Bigg)\int_{-\frac{h}{2}}^{\frac{h}{2}}f(z)dz$$
$$+\Bigg(\nu_{12}E_{2}\Bigg(-\frac{1}{r}\frac{dw_{i}}{dr}+y^{*}\frac{1}{r}\phi_{i}\Bigg)+E_{1}\Bigg(-\frac{d^{2}w_{i}}{dr^{2}}+y^{*}\frac{d\phi_{i}}{dr}\Bigg)\Bigg)\int_{-\frac{h}{2}}^{\frac{h}{2}}zf(z)dz+ \tag{34}$$
$$\Bigg(E_{1}\frac{d\phi_{i}}{dr}+\nu_{12}E_{2}\frac{1}{r}\phi_{i}\Bigg)\int_{-\frac{h}{2}}^{\frac{h}{2}}(f(z))^{2}dz\Bigg)\Bigg\}$$

$$R_{i\theta}^{L}=(1-l^{2}\nabla^{2})\Bigg\{\frac{E_{2}}{1-\nu_{12}\nu_{21}}\Bigg(\Bigg(\nu_{12}\Bigg(\frac{du_{i}}{dr}+\frac{1}{2}\Big(\frac{dw_{i}}{dr}\Big)^{2}\Bigg)+\frac{1}{r}u_{i}\Bigg)\int_{-\frac{h}{2}}^{\frac{h}{2}}f(z)dz+$$
$$\Bigg(\nu_{12}\Bigg(-\frac{d^{2}w_{i}}{dr^{2}}+y^{*}\frac{d\phi_{i}}{dr}\Bigg)+\Bigg(-\frac{1}{r}\frac{dw_{i}}{dr}+y^{*}\frac{1}{r}\phi_{i}\Bigg)\Bigg)\int_{-\frac{h}{2}}^{\frac{h}{2}}zf(z)dz+ \tag{35}$$
$$\Bigg(\nu_{12}\frac{d\phi_{i}}{dr}+\frac{1}{r}\phi_{i}\Bigg)\int_{-\frac{h}{2}}^{\frac{h}{2}}(f(z))^{2}dz\Bigg)\Bigg\}$$

$$Q_{ir}^{L}=(1-l^{2}\nabla^{2})\Bigg\{G_{13}\phi_{i}y^{*}h+G_{13}\phi_{i}\int_{-\frac{h}{2}}^{\frac{h}{2}}(f'(z)+y^{*})dz\Bigg\} \tag{36}$$

$$R_{irz}^{L}=(1-l^{2}\nabla^{2})\Bigg\{G_{13}\phi_{i}\int_{-\frac{h}{2}}^{\frac{h}{2}}(f'(z))^{2}dz+G_{13}y^{*}\phi_{i}\int_{-\frac{h}{2}}^{\frac{h}{2}}f'(z)dz\Bigg\} \tag{37}$$

For the first layer ($i = 1$) and the subsequent layers, the equilibrium relationships (local form) are explained as follows:

$$\delta u_{i}:Ni_{r}^{L}+r\frac{dNi_{r}^{L}}{dr}-Ni_{\theta}^{L}=0\ ,\ i=1,\dots n \tag{38}$$

$$\begin{gathered}\delta w_{1}:r\tfrac{d^{2}M_{1r}^{L}}{dr^{2}}+2\tfrac{dM_{1r}^{L}}{dr}-\tfrac{dM_{1\theta}^{L}}{dr}+\big(1-\mu\nabla^{2}\big)\big((q+k_{0}(w_{2}-w_{1}))r+\\ N_{1\theta}^{L}\tfrac{dw_{1}}{dr}+rN_{1r}^{L}\tfrac{d^{2}w_{1}}{dr^{2}}\Big)+\mu r\Big(\big(\nabla^{2}N_{1r}^{L}\big)\tfrac{d^{2}w_{1}}{dr^{2}}+\big(\nabla^{2}N_{1\theta}^{L}\big)\tfrac{1}{r}\tfrac{dw_{1}}{dr}\Big)=0\end{gathered} \tag{39}$$

$$\begin{gathered}\delta w_{i}:r\tfrac{d^{2}M_{ir}^{L}}{dr^{2}}+2\tfrac{dM_{ir}^{L}}{dr}-\tfrac{dM_{i\theta}^{L}}{dr}+\big(1-\mu\nabla^{2}\big)\big((-k_{0}(w_{i}-w_{i-1})+k_{0}(w_{i}-w_{i-1}))r+\\ N_{i\theta}^{L}\tfrac{dw_{i}}{dr}+rN_{ir}^{L}\tfrac{d^{2}w_{i}}{dr^{2}}\Big)=0,\ (i=2,\dots n-1)\end{gathered} \tag{40}$$

$$\begin{gathered}\delta w_{n}:r\tfrac{d^{2}M_{nr}^{L}}{dr^{2}}+2\tfrac{dM_{nr}^{L}}{dr}-\tfrac{dM_{n\theta}^{L}}{dr}+\big(1-\mu\nabla^{2}\big)\big((-k_{0}(w_{n}-w_{n-1})-k_{w}w_{n}+k_{p}\nabla^{2}w_{n})r+\\ N_{n\theta}^{L}\tfrac{dw_{2}}{dr}+rN_{nr}^{L}\tfrac{d^{2}w_{n}}{dr^{2}}\Big)=0\end{gathered} \tag{41}$$

$$\delta\phi_{i}:y^{*}\Bigg(r\frac{dM_{ir}^{L}}{dr}+M_{ir}^{L}-M_{i\theta}^{L}-rQ_{ir}^{L}\Bigg)+R_{ir}^{L}+r\frac{dR_{ir}^{L}}{dr}-R_{i\theta}^{L}-rR_{irz}^{L}=0,i=1,\dots n \tag{42}$$

Also for the buckling analysis of the circular (or annular) nanoplate, the stability equations are as follows:

$$\delta u_{i}:Ni_{r}^{L}+r\frac{dNi_{r}^{L}}{dr}-Ni_{\theta}^{L}=0\ ,\ i=1,\dots n \tag{43}$$

$$\begin{array}{l}\delta w_1 : r\frac{d^2M_{1r}^L}{dr^2} + 2\frac{dM_{1r}^L}{dr} - \frac{dM_{1\theta}^L}{dr} + \\ \left(1-\mu\nabla^2\right)\left((k_0(w_2-w_1))r + N_{1\theta}^L\frac{dw_1}{dr} + rN_{1r}^L\frac{d^2w_1}{dr^2} - \overline{N}\left(\frac{dw_1}{dr} + r\frac{d^2w_1}{dr^2}\right) + \right. \\ \left.\mu\left(\left(\nabla^2N_{1r}^L\right)\frac{\partial^2w_1}{\partial r^2} + \left(\nabla^2N_{1\theta}^L\right)\left(\frac{1}{r}\frac{\partial w_1}{\partial r}\right)\right)\right) = 0\end{array} \tag{44}$$

$$\begin{array}{l}\delta w_i : r\frac{d^2M_{ir}^L}{dr^2} + 2\frac{dM_{ir}^L}{dr} - \frac{dM_{i\theta}^L}{dr} + \left(1-\mu\nabla^2\right)((-k_0(w_i-w_{i-1}))r + N_{i\theta}^L\frac{dw_i}{dr} + \\ rN_{ir}^L\frac{d^2w_i}{dr^2} - \overline{N}\left(\frac{dw_i}{dr} + r\frac{d^2w_i}{dr^2}\right) + \mu\left(\left(\nabla^2N_{ir}^L\right)\frac{\partial^2w_i}{\partial r^2} + \left(\nabla^2N_{i\theta}^L\right)\right)\left(\frac{1}{r}\frac{\partial w_i}{\partial r}\right)\Big) = 0,\ (i = 2\ldots n-1)\end{array} \tag{45}$$

$$\begin{array}{l}\delta w_n : r\frac{d^2M_{nr}^L}{dr^2} + 2\frac{dM_{nr}^L}{dr} - \frac{dM_{n\theta}^L}{dr} + \left(1-\mu\nabla^2\right)\left(\left(-k_0(w_n-w_{n-1}) - k_ww_n + k_p\nabla^2w_n\right)r + \right. \\ \left. N_{n\theta}^L\frac{dw_n}{dr} + rN_{nr}^L\frac{d^2w_n}{dr^2}\right) = 0\end{array} \tag{46}$$

$$\delta\phi_i : y^*\left(r\frac{dM_{ir}^L}{dr} + M_{ir}^L - M_{i\theta}^L - rQ_{ir}^L\right) + R_{ir}^L + r\frac{dR_{ir}^L}{dr} - R_{i\theta}^L - rR_{irz}^L = 0, i = 1,\ldots n \tag{47}$$

Moreover, it is possible to obtain the equilibrium relationships for the multilayer sector plate. In that case, the displacement field (considering the HSDT) can be expressed as follows (ψ is the rotation components in the r direction.):

$$\begin{array}{l}U_i(r,\theta,z) = u_i(r,\theta) - z\frac{\partial w_i(r,\theta)}{\partial r} + g(z)\phi_i(r,\theta)\ ,\ i = 1,\ldots n \\ V_i(r,\theta,z) = v_i(r,\theta) - \frac{z}{r}\frac{\partial w_i(r,\theta)}{\partial\theta} + g(z)\psi_i(r,\theta)\ ,\ i = 1,\ldots n \\ W_i(r,\theta,z) = w_i(r,\theta)\ ,\ i = 1,\ldots n\end{array} \tag{48}$$

Therefore, the equilibrium relationships are as follows:

$$\delta u_i : Ni_r^L - Ni_\theta^L + r\frac{\partial Ni_r^L}{\partial r} + \frac{\partial Ni_{r\theta}^L}{\partial\theta} = 0\ ,\ i = 1,\ldots n \tag{49}$$

$$\delta v_i : \frac{\partial Ni_\theta^L}{\partial\theta} + r\frac{\partial Ni_{r\theta}^L}{\partial r} + 2Ni_{r\theta}^L = 0\ ,\ i = 1,\ldots n \tag{50}$$

$$\begin{array}{l}\delta w_1 : r\frac{\partial^2M_{1r}^L}{\partial r^2} + 2\frac{\partial M_{1r}^L}{\partial r} - \frac{\partial M_{1\theta}^L}{\partial r} + \frac{1}{r}\frac{\partial^2M_{1\theta}^L}{\partial\theta^2} + \frac{2}{r}\frac{\partial M_{1r\theta}^L}{\partial\theta} + \\ 2\frac{\partial^2M_{1r\theta}^L}{\partial\theta\partial r} + \left(1-\mu\nabla^2\right)((q + k_0(w_2-w_1))r + N_{1\theta}^L\frac{\partial w_1}{\partial r} + \\ rN_{1r}^L\frac{\partial^2w_1}{\partial r^2} + \frac{1}{r}N_{1\theta}\frac{\partial^2w_1}{\partial\theta^2} + \frac{1}{r}\frac{\partial N_{1\theta}^L}{\partial\theta}\frac{\partial w_1}{\partial\theta} + \frac{\partial N_{1r\theta}^L}{\partial r}\frac{\partial w_1}{\partial\theta} + \\ 2N_{1r\theta}^L\frac{\partial^2w_1}{\partial r\partial\theta}\Big) + \mu r\Big(\left(\nabla^2N_{1r}^L\right)\frac{\partial^2w_1}{\partial r^2} + \left(\nabla^2N_{1\theta}^L\right)\left(\frac{1}{r}\frac{\partial w_1}{\partial r} + \frac{1}{r^2}\frac{\partial^2w_1}{\partial\theta^2}\right) + \\ 2\left(\nabla^2N_{1r\theta}^L\right)\left(\frac{1}{r}\frac{\partial^2w_1}{\partial r\partial\theta} - \frac{1}{r^2}\frac{\partial w_1}{\partial\theta}\right)\Big) = 0\end{array} \tag{51}$$

$$\begin{array}{l}\delta w_i : r\frac{\partial^2M_{ir}^L}{\partial r^2} + 2\frac{\partial M_{ir}^L}{\partial r} - \frac{\partial M_{i\theta}^L}{\partial r} + \frac{1}{r}\frac{\partial^2M_{i\theta}^L}{\partial\theta^2} + \\ \frac{2}{r}\frac{\partial M_{ir\theta}^L}{\partial\theta} + 2\frac{\partial^2M_{ir\theta}^L}{\partial\theta\partial r} + \\ \left(1-\mu\nabla^2\right)((-k_0(w_i-w_{i-1}))r + \\ N_{i\theta}^L\frac{\partial w_i}{\partial r} + rN_{ir}^L\frac{\partial^2w_i}{\partial r^2} + \frac{1}{r}N_{2\theta}\frac{\partial^2w_i}{\partial\theta^2} + \frac{1}{r}\frac{\partial N_{i\theta}^L}{\partial\theta}\frac{\partial w_i}{\partial\theta} + \\ \frac{\partial N_{ir\theta}^L}{\partial r}\frac{\partial w_i}{\partial\theta} + 2N_{ir\theta}^L\frac{\partial^2w_i}{\partial r\partial\theta} + \\ \mu r\Big(\left(\nabla^2N_{ir}^L\right)\frac{\partial^2w_i}{\partial r^2} + \left(\nabla^2N_{i\theta}^L\right)\left(\frac{1}{r}\frac{\partial w_i}{\partial r} + \frac{1}{r^2}\frac{\partial^2w_i}{\partial\theta^2}\right) + \\ 2\left(\nabla^2N_{ir\theta}^L\right)\left(\frac{1}{r}\frac{\partial^2w_i}{\partial r\partial\theta} - \frac{1}{r^2}\frac{\partial w_i}{\partial\theta}\right)\Big) = 0\ ,\ (i = 2\ldots,n-1)\end{array} \tag{52}$$

$$\begin{aligned}
&\delta w_n : r\tfrac{\partial^2 M^L_{nr}}{\partial r^2} + 2\tfrac{\partial M^L_{nr}}{\partial r} - \tfrac{\partial M^L_{n\theta}}{\partial r} + \tfrac{1}{r}\tfrac{\partial^2 M^L_{n\theta}}{\partial \theta^2} + \\
&\tfrac{2}{r}\tfrac{\partial M^L_{nr\theta}}{\partial \theta} + 2\tfrac{\partial^2 M^L_{nr\theta}}{\partial \theta \partial r} + \\
&\left(1-\mu\nabla^2\right)\left(\left(-k_0(w_n - w_{n-1}) - k_w w_n + k_p\nabla^2 w_n\right)r + \right. \\
&N^L_{n\theta}\tfrac{\partial w_n}{\partial r} + rN^L_{nr}\tfrac{\partial^2 w_n}{\partial r^2} + \tfrac{1}{r}N_2 n\tfrac{\partial^2 w_n}{\partial \theta^2} + \tfrac{1}{r}\tfrac{\partial N^L_{n\theta}}{\partial \theta}\tfrac{\partial w_n}{\partial \theta} + \\
&\tfrac{\partial N^L_{nr\theta}}{\partial r}\tfrac{\partial w_n}{\partial \theta} + 2N^L_{nr\theta}\tfrac{\partial^2 w_n}{\partial r \partial \theta} + \\
&\mu r\Big(\left(\nabla^2 N^L_{nr}\right)\tfrac{\partial^2 w_n}{\partial r^2} + \left(\nabla^2 N^L_{n\theta}\right)\left(\tfrac{1}{r}\tfrac{\partial w_n}{\partial r} + \tfrac{1}{r^2}\tfrac{\partial^2 w_n}{\partial \theta^2}\right) + \\
&\left.2\left(\nabla^2 N^L_{nr\theta}\right)\left(\tfrac{1}{r}\tfrac{\partial^2 w_n}{\partial r \partial \theta} - \tfrac{1}{r^2}\tfrac{\partial w_n}{\partial \theta}\right)\Big)\right) = 0
\end{aligned} \tag{53}$$

$$\begin{aligned}
&\delta\phi_i : y^*\left(r\tfrac{\partial Mi^L_r}{\partial r} + \tfrac{\partial Mi^L_{r\theta}}{\partial \theta} + Mi^L_r - Mi^L_\theta - rQi^L_r\right) + \\
&Ri^L_r - Ri^L_\theta + r\tfrac{\partial Ri^L_r}{\partial r} + \tfrac{\partial Ri^L_{r\theta}}{\partial \theta} - rRi^L_{rz} = 0 \ , \ i = 1, \ldots n
\end{aligned} \tag{54}$$

$$\begin{aligned}
&\delta\psi_i : y^*\left(r\tfrac{\partial Mi^L_{r\theta}}{\partial r} + \tfrac{\partial Mi^L_\theta}{\partial \theta} + 2Mi^L_{r\theta} - rQi^L_\theta\right) + 2Ri^L_{r\theta} - \\
&rRi^L_{z\theta} + r\tfrac{\partial Ri^L_{r\theta}}{\partial r} + \tfrac{\partial Ri^L_\theta}{\partial \theta} = 0 \ , \ i = 1, \ldots n
\end{aligned} \tag{55}$$

Also, the boundary conditions of the present study for the circular (or annular) plate can be noticed as given below:

Simply supported (S):

$$u_i = w_i = M_{ir} = R_{ir} = 0 \tag{56}$$

Clamped (C):

$$u_i = w_i = \phi_i = \frac{dw_i}{dr} = 0 \tag{57}$$

Free (F):

$$N_{ir} = M_{ir} = R_{ir} = Q_{ir} = 0 \tag{58}$$

Also, the boundary condition of the sector plate in the clamped (C) condition is as follows:

$$\begin{aligned}
&u = v = w = \varphi = \psi = 0 \; r = r_i \ , \ r_o \\
&u = v = w = \varphi = \psi = 0 \; \theta = 0 \ , \ \tau
\end{aligned} \tag{59}$$

Moreover, for converting the governing mathematical relationships of the dimensionless nanoplate, the following assumptions are considered:

$$\begin{aligned}
&u^* = \tfrac{u_0}{h} \ ; \ w^* = \tfrac{w_0}{r_o} \ ; \ \phi^* = \phi \ ; \psi^* = \psi \ ; \ N^*_r = \tfrac{N_r}{E_1 h} \ ; \ N^*_\theta = \tfrac{N_\theta}{E_1 h}; \\
&Q^*_r = \tfrac{Q_r}{E_1 h} \ ; \ Q^*_\theta = \tfrac{Q_\theta}{E_1 h} \ ; \ M^*_r = \tfrac{M_r}{E_1 h^2} \ ; \ M^*_\theta = \tfrac{M_\theta}{E_1 h^2} \ ; \ \nabla^{*2} = \tfrac{d^2}{dr^{*2}} + \tfrac{1}{r^*}\tfrac{d}{dr^*}; \\
&R^*_r = \tfrac{R_r}{E_1 h^2} \ ; \ R^*_\theta = \tfrac{R_\theta}{E_1 h^2} \ ; \ R^*_{rz} = \tfrac{R_{rz}}{E_1 h} \ ; \ r^* = \tfrac{r}{r_o} \ ; \ z^* = \tfrac{z}{h} \ ; \\
&\delta = \tfrac{h}{r_o} \ ; \ \mu^* = \tfrac{\mu}{r_o^2} \ ; \ l^* = \tfrac{l}{r_o} \ ; \ q^* = \tfrac{q}{E_1} \ ; k^*_w = \tfrac{k_w r_o}{E_1} \ ; \ k^*_p = \tfrac{k_p}{E_1 r_o}
\end{aligned} \tag{60}$$

3. Numerical Solution Method

Considering the definition of polynomials, the semi–analytical polynomial technique is a straightforward approach for solving both ordinary and partial differential mathematical relationships. In this study for obtaining the results of circular/annular plates, SAPM is used.

The differential equations can be changed to an algebraic equation system by replacing u^*, w^*, and φ^* as functions in equilibrium equations:

$$\begin{aligned}
u^* &= \sum_{i=1}^{N} a_i r^{(i-1)} \\
w^* &= \sum_{i=1}^{N} a_{(i+N)} r^{(i-1)} \\
\varphi^* &= \sum_{i=1}^{N} a_{(i+2N)} r^{(i-1)}
\end{aligned} \tag{61}$$

There are currently N unknown constants and N algebraic equations. Then, using a numerical technique (for example the Newton-Raphson method), this set of algebraic equations can be solved (Please see the Appendix A for more details).

The extended Kantorovich method (EKM) was created by Arnold Kerr [51] and is one of the efficient techniques to solve partial differential mathematical relationships. In this paper, first, the 2D equations of the sector plate are converted into one-dimensional form via the extended Kantorovich technique. Then DQM is used to solve the equations.

Using the EKM, the product of univariate functions can be obtained as [51]:

$$f(r,\theta) = f_1(r) \times g_1(\theta) \tag{62}$$

So, the displacement and rotation functions are as follows:

$$u(r,\theta) = f_1(r) \times g_1(\theta) \tag{63}$$

$$v(r,\theta) = f_2(r) \times g_2(\theta) \tag{64}$$

$$w(r,\theta) = f_3(r) \times g_3(\theta) \tag{65}$$

$$\phi(r,\theta) = f_4(r) \times g_4(\theta) \tag{66}$$

$$\psi(r,\theta) = f_5(r) \times g_5(\theta) \tag{67}$$

By inserting Equations (63)–(67) in the equilibrium equations, ordinary differential equations are obtained. Then choosing the arbitrary initial of $g_i, i = 1 \ldots 5$, the equations can be derived with the weighted Galerkin residual technique. Therefore, the governing mathematical relationships are then multiplied by an appropriate function, and after integration, ordinary differential equations can be derived, which is a function of $f_i, i = 1 \ldots 5$. Then, by solving these equations, the f_i functions can be derived [51]:

$$\int_0^\tau g_1(\theta) \times e_1 d\theta = 0 \tag{68}$$

$$\int_0^\tau g_2(\theta) \times e_2 d\theta = 0 \tag{69}$$

$$\int_0^\tau g_3(\theta) \times e_3 d\theta = 0 \tag{70}$$

$$\int_0^\tau g_4(\theta) \times e_4 d\theta = 0 \tag{71}$$

$$\int_0^\tau g_5(\theta) \times e_5 d\theta = 0 \tag{72}$$

where, $e_1, e_2, \ldots, e_5$ are equilibrium mathematical relationships.

Each equilibrium equation must be multiplied by the appropriate g_i and integrated from 0 to τ. By inserting the obtained f_i functions in the equilibrium equations, the ordinary differential equations are obtained, from which the differential relationships can be solved to calculate g_i.

Partial differential equations can be single-variable using the introduced functions and become ordinary types. For the numerical solution of one-dimensional differential relationships, DQM is among the most effective methods. DQM is defined as one node's integral along the domain, which is dependent upon every other node in that direction [52]:

$$\left.\frac{df}{dr}\right|_{r_i} = \sum_{j=1}^{N} A_{ij} f(r_j) \; , i = 1, 2, \ldots, N \tag{73}$$

In the above relationship (Equation (73)), weight coefficients as well as function values at discrete nodes are determined with $w_1, w_2, \ldots, w_n$ and $f_1, f_2, \ldots, f_n$.

The author of ref. [53] reported that in quadratic form, the derivative at a specific node in the function domain depends on the function values of each node in the domain through the weight parameter:

$$A_{ij}^{(1)} = \frac{P(r_i)}{(r_i - r_j)P(r_j)} \tag{74}$$

$$P(r_i) = \prod_{j=1}^{N}(r_i - r_j)\ , i \neq j \tag{75}$$

$$A_{ii}^{(1)} = -\sum_{k=1}^{N} A_{ik}^{(1)}\ , i \neq k \tag{76}$$

Moreover, for the higher-order derivatives, the Equation (77) can be expressed as follows [52]:

$$\left.\frac{d^{(n)}f}{dr^{(n)}}\right|_{r_i} = \sum_{j=1}^{N} A_{ij}^{(n)} f(r_j)\ , i = 1, \ldots, N \tag{77}$$

For higher derivatives, the weighting coefficients are as given below [52]:

$$A_{ij}^{(n)} = n\left[A_{ij}^{(1)} A_{ii}^{(n-1)} - \frac{A_{ij}^{(n-1)}}{(r_i - r_j)}\right]\ , i \neq j \tag{78}$$

$$A_{ii}^{(n)} = -\sum_{j=1,\neq i}^{N} A_{ij}^{(n)}\ , i, j = 1 \ldots N \tag{79}$$

where N can be defined as the number of grid points in the direction of r. To obtain more precise results, it is more recommended to use the grid point distribution, which is based on Chebyshev–Gauss–Lobatto points. Based on the distribution of Chebyshev–Gauss–Lobatto grid points, the grid points' coordinates can be written as follows [52]:

$$r_i = \frac{a}{2}\left[1 - \cos\left(\frac{\pi i}{N-1}\right)\right], i = 0, 1, \ldots, N \tag{80}$$

4. Results and Discussion

This section examines the static behavior of the circular (or annular) and sector nanoplates via HSDT. The nonlocal strain gradient model is taken into account using SAPM. Additionally, the current results are contrasted with the references' results in order to validate the solution approach.

Figure 3 illustrates how the number of nodes (N) in the solution method affects the current study's findings. Proper convergence is attained after nine nodes, as is shown.

Table 2 compares the deflection of the single-layer circular nanoplate with references via the following assumptions:

$$E_1 = E_2 = 2 \times 10^6 \text{ Pa}, \mu = 0, \nu_{12} = \nu_{21} = 0.3, R^* = \frac{r_0}{h} = 10 \tag{81}$$

In this part, several functions are gathered to define the shear stress distribution along the thickness:

$$\begin{aligned} &g_1(z) = \tfrac{h}{\pi}\sin\left(\tfrac{\pi z}{h}\right), g_2(z) = -\tfrac{4}{3h^2}z^3 + z, g_3(z) = h\sinh\left(\tfrac{z}{h}\right) - z\cosh\left(\tfrac{1}{2}\right), \\ &g_4(z) = ze^{-2\left(\frac{z}{h}\right)^2}, g_5(z) = -\tfrac{5}{3h^2}z^3 + \tfrac{5}{4}z \end{aligned} \tag{82}$$

As can be seen from comparison with Table 2, the outcomes of this part are in acceptable harmony with the outcome of the previous papers. Also, the results of using different values of g(z) interchangeably are actually negligible when compared to other parameters.

Therefore, it is optional to use any types of g(z) functions introduced in Table 1 to obtain the results.

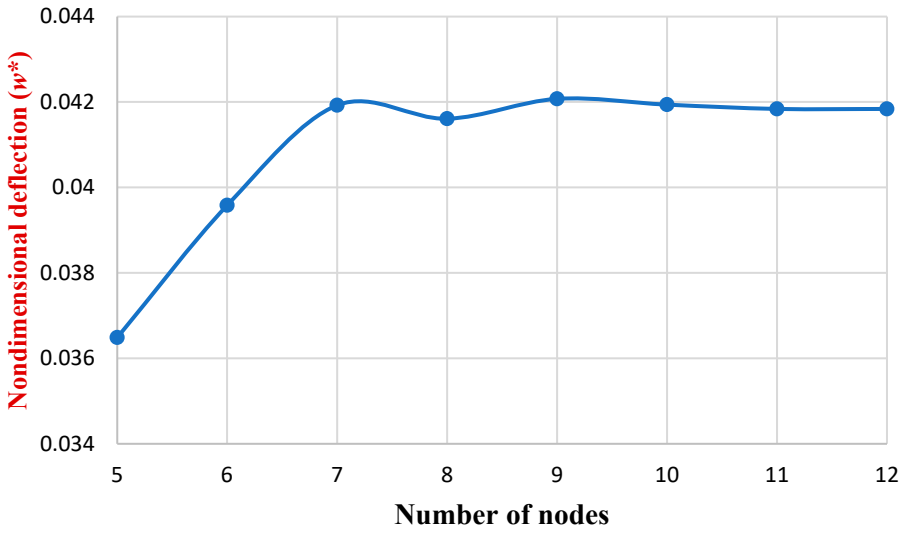

Figure 3. The convergence of the solution method in terms of the grid points (N).

Table 2. The non-dimensional maximum deflection of the single-layer circular plate compared to the references for different values of nondimensional load (q^*).

q^*	Ref. [54]	Ref. [55]	Ref. [56]	Present (g1)	Present (g2)	Present (g3)	Present (g4)	Present (g5)
0.0001	0.1678	0.1687	0.1706	0.1732	0.1801	0.1793	0.1789	0.1801
0.0003	0.4583	0.4655	0.5119	0.471	0.4863	0.4843	0.4835	0.4863
0.001	1.0509	1.0937	1.7069	1.0708	1.0929	1.0899	1.0887	1.0929

Table 3 compares the deflections gathered by the authors with those documented in the paper [57] for the single-layer sector plate, considering Equation (83):

$$\tau = \frac{\pi}{3},\ E = 200 \times 10^9 \text{Pa},\ q = 1\text{Pa},\ \frac{r}{h} = 100 \tag{83}$$

Table 3. The deflection obtained by the authors compared to the reference for the sector plate.

r_i/r_o	[57]	Present Study
0.25	2.84	2.85
0.5	1.41	1.45
0.75	0.1	0.093

It is noticed that the results obtained by the authors are in good harmony with the reference.

The following definition of buckling strain is used for validation purposes [41,58]:

$$\varepsilon_b = \frac{\overline{N}}{Eh} \tag{84}$$

where ε_b is strain buckling and $\overline{N}$ is buckling load. Also E and h are the Young modulus and thickness given in the reference. For a range of nonlocal parameters and radiuses, Table 4. lists the buckling strains of the circular nanoplate with a clamped edge. It can be noticed that the current findings closely resemble those of ref. [41].

Table 4. Nondimensional strain buckling of single-layer and bilayer circular nanoplate with clamped boundary conditions obtained by the authors with ref. [41].

Reference	r (nm)	The Percentage of the strain of Buckling		
		μ=0	μ=1	μ=4
Present single-layer	4	0.91	0.48	0.19
Present bilayer	4	1.38	0.84	0.33
Reference [41]	4	0.93	0.47	0.19
Present single-layer	8	0.23	0.19	0.12
Present bilayer	8	1.09	0.81	0.41
Reference [41]	8	0.23	0.19	0.12

Regarding the following data:

$$\begin{array}{l} E_1 = 1765(\text{GPa}) \text{ , } E_2 = 1588(\text{GPa}) \text{ ,} \nu_{12} = 0.3 \text{ , } \nu_{21} = 0.27, \ q = 1(\text{GPa}) \text{ ,} \\ k_0 = 50(\text{GPa/nm}), k_w = 1.13(\text{GPa/nm}), k_p = 1.13(\text{Pa.m}), h = 0.34(\text{nm}) \text{ ,} \\ r_i = 10(\text{nm}), r_o = 10(\text{nm}). \end{array} \quad (85)$$

the results of the current study are examined. Figure 4a,b show the results of the nondimensional maximum deflection versus the van der Waals coefficient between layers for the annular multi-layer nanoplate (i = 2) at different boundary conditions. With the enhancement of the van der Waals coefficient between layers, the maximum deflection decreases. By increasing the van der Waals coefficient between layers, the stiffness of the nanoplates is enhanced, and as a result, the dimensionless deflection of the plates is reduced. Despite the single–layer plate deflection behavior, it is noticed that the maximum nondimensional deflection for the simply supported boundary condition is more than that of the clamped boundary condition. Also, it is concluded that increasing the nonlocal parameter decreases the deflection of the plate.

By considering the Equation (86) assumptions:

$$\begin{array}{l} E_1 = E_2 = 1.06 \times 10^{12}(\text{Pa}) \text{ , } \nu_{12} = 0.3 \text{ , } \nu_{21} = 0.27, \ q = 5(\text{GPa}) \text{ ,} \\ k_0 = 50(\text{GPa/nm}), k_w = 1.13(\text{GPa/nm}), k_p = 1.13(\text{Pa.m}), h = 0.34(\text{nm}) \text{ ,} \\ r_i = 10(\text{nm}), r_o = 10(\text{nm}) \end{array} \quad (86)$$

the results of the sector analysis are examined. Figure 5. compares the results of the maximum deflection of the multi-layer sector nanoplate (i = 2) with an equivalent single-layer plate (with the same thickness as the multi-layer one) versus the sector angle in the clamped condition. Moreover, it can be noticed that by increasing the strain gradient parameter, the maximum dimensionless deflection of the plate decreases. This reduction is made more significant by increasing the sector angle. Additionally, increasing the sector angle causes an increase in the deflection of the plate.

Figure 6 reveals the nondimensional buckling load of the circular multilayer nanoplate (i = 2) with respect to the thickness-to-radius ratio (h/r) for the clamped and simply supported boundary conditions. From the graph, it is evident that increasing the h/r decreases the nondimensional buckling load. Also, by increasing the h/r, the outcomes of the clamped and simply supported boundary conditions approach each other.

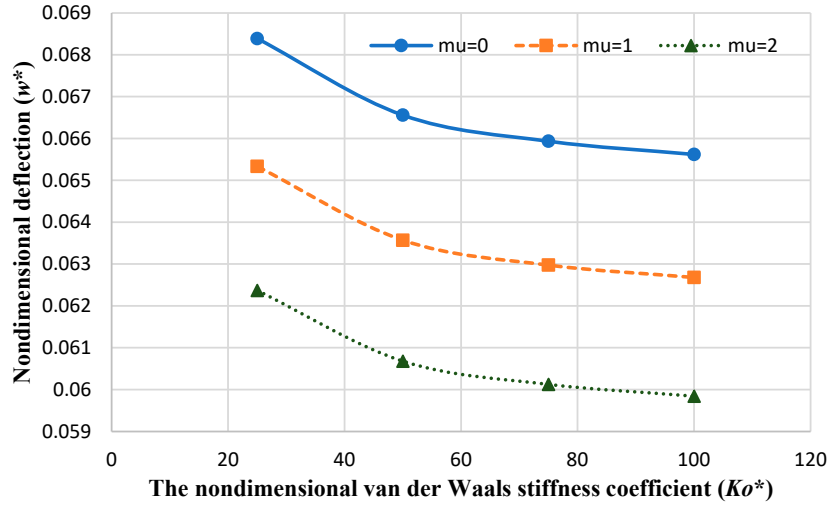

(**a**)

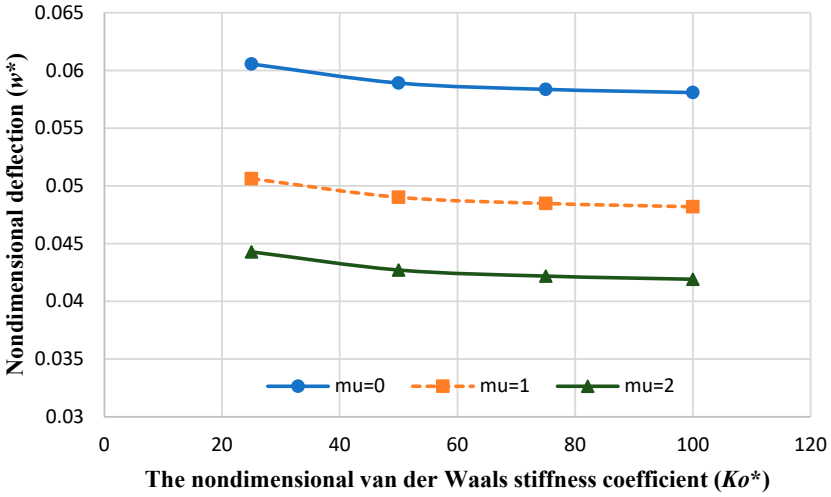

(**b**)

Figure 4. (**a**) The deflection of the annular multi-layer nanoplate (i = 2) versus the van der Waals coefficient among layers in the S-F boundary condition. (**b**) The deflection of the annular multi-layer nanoplate (n = 2) versus the van der Waals coefficient among layers in the C-F boundary condition.

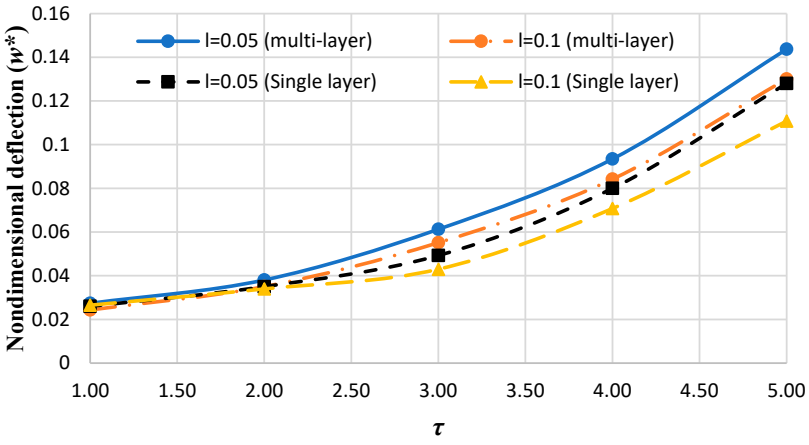

Figure 5. The comparison of the maximum nondimensional deflection of the multi-layer sector nanoplate (i = 2) with equivalent single-layer plate versus the sector angle in the clamped boundary condition.

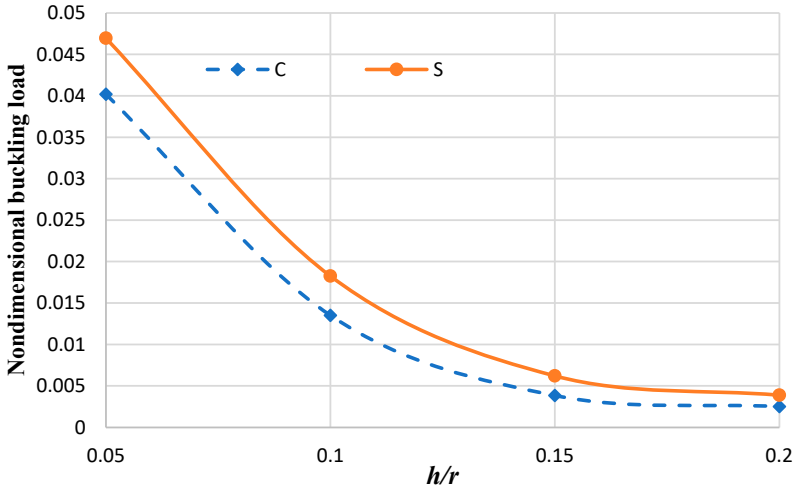

Figure 6. The buckling load of the circular multilayer nanoplate (i = 2) with respect to the thickness-to-radius ratio.

5. Conclusions

The static examination of the circular (or annular) and sector multi-layer nanoplate via the nonlocal strain gradient theory with HSDT considering nonlinear strains, was carried out herein. Additionally, the mechanical buckling of the multi-layer sector nanoplate was studied. Also, to solve governing mathematical relations, SAPM and DQM were used. For validation, other references were used to compare the results. Examinations were carried out to study the effect of small-scale factors, the van der Waals interaction value among layers, boundary conditions, and geometric factors of the plate.

Author Contributions: M.S., conceptualization, methodology, software, validation, formal analysis, investigation, and writing—original draft preparation; A.P., supervision, conceptualization, methodology, and formal analysis; P.G., investigation; G.J., validation and investigation. All authors have read and agreed to the published version of the manuscript.

Funding: This research received no external funding.

Data Availability Statement: Data are contained within the article.

Conflicts of Interest: The authors declare no conflict of interest.

Appendix A

For the bending analysis, by using SAPM and placing the polynomial functions of Equation (61) in the equilibrium equations (obtained based on displacements), the differential mathematical relationships are converted to an algebraic mathematical equations system. Also, instead of SAPM, it is possible to use DQM to discretize the differential equations and convert them to series form. Then, using numerical methods such as Newton–Raphson, these algebraic equations can be solved. In this type of analysis, there are N unknown constants and N algebraic equations.

For the buckling analysis, either SAPM or DQM can be used to convert them to algebraic equations. In this type of analysis, there are N algebraic equations and $N + 1$ unknown constants. Therefore, the Newton–Raphson method cannot be solely used to obtain the results. For this type of analysis, the methods of eigenvalues and eigenvectors can be used.

For example, consider the buckling of the single-layer circular plate using first-order shear deformation theory. Therefore, for each node, there are four unknowns and three equations, whose unknowns are, e.g., w_0, φ, u_0 (displacement components of the middle plate) and $\overline{N}$ (critical buckling load). So, there are 34 unknowns and 33 equations for 11 nodes. After discretizing the equilibrium equations (using SAPM or DQM) and sub-

stituting displacements in them, the matrix form of the obtained equations is generally expressed as follows:

$$[Cef]_{33*33}\begin{Bmatrix} u_0^{*1} \\ \varphi^{*1} \\ w_0^{*1} \\ . \\ . \\ u_0^{*11} \\ \varphi^{*11} \\ w_0^{*11} \end{Bmatrix} = 0 \tag{A1}$$

$[Cef]_{33*33}$ is the matrix of coefficients of obtained equations for 11 nodes. By setting the determinant of the matrix of coefficients equal to zero in the computer program (using MATLAB 8.4 R2014b, Maple 2023, etc.), the critical buckling load can be obtained. This technique is also can be used for solving equations in higher-order theories with more displacements and equations.

Also, the iteration method can be applied by guessing the buckling load solving the equations (as the bending analysis), and checking the deflection of the plate:

$$\frac{\left|\overline{N}^{r+1} - \overline{N}^{r}\right|}{\overline{N}^{r+1}} \leq \varepsilon_0 \tag{A2}$$

where ε_0 is a small value and can be taken as 10^{-4}. Also, here $r + 1$ and r show the two consequent iterations, for obtaining the critical buckling load ($\overline{N}$).

References

1. Gupta, R.; Kumar, A.; Biswas, A.; Singh, R.; Gehlot, A.; Akram, S.V.; Verma, A.S. Advances in micro and nano-engineered materials for high-value capacitors for miniaturized electronics. *J. Energy Storage* **2022**, *55*, 105591. [CrossRef]
2. Manolis, G.D.; Dineva, P.S.; Rangelov, T.; Sfyris, D. Mechanical models and numerical simulations in nanomechanics: A review across the scales. *Eng. Anal. Bound. Elem.* **2021**, *128*, 149–170. [CrossRef]
3. Schiavo, L.; Cammarano, A.; Carotenuto, G.; Longo, A.; Palomba, M.; Nicolais, L. An overview of the advanced nanomaterials science. *Inorganica Chim. Acta* **2024**, *559*, 121802. [CrossRef]
4. Srivastava, A.K.; Tawale, J.S.; Verma, R.; Agarwal, D.; Sharma, C.; Kumar, A.; Gupta, M.K. Morphological evolution driven semiconducting nanostructures for emerging solar, biological and nanogenerator applications. *Mater. Adv.* **2022**, *3*, 8030–8062. [CrossRef]
5. Yusaf, T.; Mahamude, A.S.; Farhana, K.; Harun, W.S.; Kadirgama, K.; Ramasamy, D.; Kamarulzaman, M.K.; Subramonian, S.; Hall, S.; Dhahad, H.A. A Comprehensive Review on Graphene Nanoparticles: Preparation, Properties, and Applications. *Sustainability* **2022**, *14*, 12336. [CrossRef]
6. Roudbari, M.A.; Jorshari, T.D.; Lü, C.; Ansari, R.; Kouzani, A.Z.; Amabili, M. A review of size-dependent continuum mechanics models for micro- and nano-structures. *Thin-Walled Struct.* **2022**, *170*, 108562. [CrossRef]
7. Eringen, A.C. Nonlocal polar elastic continua. *Int. J. Eng. Sci.* **1972**, *10*, 1–16. [CrossRef]
8. Yang, F.; Chong, A.C.M.; Lam, D.C.C.; Tong, P. Couple stress based strain gradient theory for elasticity. *Int. J. Solids Struct.* **2002**, *39*, 2731–2743. [CrossRef]
9. Lam, D.C.; Yang, F.; Chong, A.; Wang, J.; Tong, P. Experiments and theory in strain gradient elasticity. *J. Mech. Phys. Solids* **2003**, *51*, 1477–1508. [CrossRef]
10. Zhu, X.; Li, L. Closed form solution for a nonlocal strain gradient rod in tension. *Int. J. Eng. Sci.* **2017**, *119*, 16–28. [CrossRef]
11. Mindlin, R.D. Micro-structure in linear elasticity. *Arch. Ration. Mech. Anal.* **1964**, *16*, 51–78. [CrossRef]
12. Tian, Y.; Xu, B.; Yu, D.; Ma, Y.; Wang, Y.; Jiang, Y.; Hu, W.; Tang, C.; Gao, Y.; Luo, K.; et al. Ultrahard nanotwinned cubic boron nitride. *Nature* **2013**, *493*, 385–388. [CrossRef] [PubMed]
13. Lim, C.W.; Zhang, G.; Reddy, J.N. A higher-order nonlocal elasticity and strain gradient theory and its applications in wave propagation. *J. Mech. Phys. Solids* **2015**, *78*, 298–313. [CrossRef]
14. Trabelssi, M.; El-Borgi, S.; Friswell, M.I. Application of nonlocal strain gradient theory for the analysis of bandgap formation in metamaterial nanobeams. *Appl. Math. Model.* **2024**, *127*, 281–296. [CrossRef]
15. Sadeghian, M.; Jamil, A.; Palevicius, A.; Janusas, G.; Naginevicius, V. The Nonlinear Bending of Sector Nanoplate via Higher-Order Shear Deformation Theory and Nonlocal Strain Gradient Theory. *Mathematics* **2024**, *12*, 1134. [CrossRef]
16. Sadeghian, M.; Palevicius, A.; Janusas, G. Nonlocal Strain Gradient Model for the Nonlinear Static Analysis of a Circular/Annular Nanoplate. *Micromachines* **2023**, *14*, 1052. [CrossRef] [PubMed]

17. Singh, B.; Jangid, K.; Mukhopadhyay, S. Implementation of Legendre wavelet method for the size dependent bending analysis of nano beam resonator under nonlocal strain gradient theory. *Comput. Math. Appl.* **2024**, *153*, 94–107. [CrossRef]
18. Xu, L.L.; Zheng, Y.F.; Chen, C.P. Nonlinear statics of magneto-electro-elastic nanoplates considering flexomagnetoelectric effect based on nonlocal strain gradient theory. *Thin-Walled Struct.* **2024**, *201*, 111974. [CrossRef]
19. Zhang, X.; Chen, B.; Shao, Z.; Ademiloye, A.S.; Yang, D.; Xiang, P.; Xianbiao, W. A size-dependent meshfree model based on nonlocal strain gradient theory for trigonometric functionally graded nanoplates on variable elastic foundations. *Structures* **2024**, *69*, 107480. [CrossRef]
20. Gui, Y.; Wu, R. Buckling analysis of embedded thermo-magneto-electro-elastic nano cylindrical shell subjected to axial load with nonlocal strain gradient theory. *Mech. Res. Commun.* **2023**, *128*, 104043. [CrossRef]
21. Lu, L.; Guo, X.; Zhao, J. A unified size-dependent plate model based on nonlocal strain gradient theory including surface effects. *Appl. Math. Model.* **2019**, *68*, 583–602. [CrossRef]
22. Arefi, M.; Kiani, M.; Rabczuk, T. Application of nonlocal strain gradient theory to size dependent bending analysis of a sandwich porous nanoplate integrated with piezomagnetic face-sheets. *Compos. Part B Eng.* **2019**, *168*, 320–333. [CrossRef]
23. Farajpour, A.; Yazdi, M.R.H.; Rastgoo, A.; Mohammadi, M. A higher-order nonlocal strain gradient plate model for buckling of orthotropic nanoplates in thermal environment. *Acta Mech.* **2016**, *227*, 1849–1867. [CrossRef]
24. Nematollahi, M.S.; Mohammadi, H. Geometrically nonlinear vibration analysis of sandwich nanoplates based on higher-order nonlocal strain gradient theory. *Int. J. Mech. Sci.* **2019**, *156*, 31–45. [CrossRef]
25. Thai, C.H.; Hung, P.T.; Nguyen-Xuan, H.; Phung-Van, P. A size-dependent meshfree approach for magneto-electro-elastic functionally graded nanoplates based on nonlocal strain gradient theory. *Eng. Struct.* **2023**, *292*, 116521. [CrossRef]
26. Thai, C.H.; Fereira, A.M.J.; Nguyen-Xuan, H.; Hung, P.T.; Phung-Van, P. A nonlocal strain gradient isogeometric model for free vibration analysis of magneto-electro-elastic functionally graded nanoplates. *Compos. Struct.* **2023**, *316*, 117005. [CrossRef]
27. Alghanmi, R.A. Nonlocal Strain Gradient Theory for the Bending of Functionally Graded Porous Nanoplates. *Materials* **2022**, *15*, 8601. [CrossRef]
28. Siddique, M.U.M.; Nazmul, I.M. Static bending analysis of BDFG nanobeams by nonlocal couple stress theory and nonlocal strain gradient theory. *Forces Mech.* **2024**, *17*, 100289. [CrossRef]
29. Phung-Van, P.; Hung, P.T.; Nguyen-Xuan, H.; Thai, C.H. Small scale analysis of porosity-dependent functionally graded triply periodic minimal surface nanoplates using nonlocal strain gradient theory. *Appl. Math. Model.* **2024**, *127*, 439–453. [CrossRef]
30. Liu, L.; Zhong, X.; Liao, S. Accurate solutions of a thin rectangular plate deflection under large uniform loading. *Appl. Math. Model.* **2023**, *123*, 241–258. [CrossRef]
31. Gao, F.; Liao, W.-H.; Wu, X. Being gradually softened approach for solving large deflection of cantilever beam subjected to distributed and tip loads. *Mech. Mach. Theory* **2022**, *174*, 104879. [CrossRef]
32. Wang, J.; Xiao, J. Analytical solutions of bending analysis and vibration of rectangular nano laminates with surface effects. *Appl. Math. Model.* **2022**, *110*, 663–673. [CrossRef]
33. Krysko, V.A.; Awrejcewicz, J.; Kalutsky, L.A.; Krysko, V.A. Quantification of various reduced order modelling computational methods to study deflection of size-dependent plates. *Comput. Math. Appl.* **2023**, *133*, 61–84. [CrossRef]
34. Al Muhammadi, M.F.S.; Al Mukahal, F.H.H.; Sobhy, M. A Higher-Order Theory for Nonlinear Dynamic of an FG Porous Piezoelectric Microtube Exposed to a Periodic Load. *Mathematics* **2024**, *12*, 3422. [CrossRef]
35. Sadeghian, M.; Pilkauskas, K.; Palevicius, P.; Ragulskiene, J.; Janusas, G.; Dorosevas, V.; Palevicius, A. A Nonlinear Damper with Dynamic Load and an Elastic Slit Membrane: Modeling and Interaction Analysis. *Appl. Sci.* **2024**, *14*, 7663. [CrossRef]
36. Cong, P.H.; Duc, N.D. Effect of nonlocal parameters and Kerr foundation on nonlinear static and dynamic stability of micro/nano plate with graphene platelet reinforcement. *Thin-Walled Struct.* **2023**, *182*, 110146. [CrossRef]
37. Wu, J.; Song, L.; Huang, K. Nonlinear static behaviors of nonlocal nanobeams incorporating longitudinal linear temperature gradient. *Int. J. Therm. Sci.* **2025**, *208*, 109421. [CrossRef]
38. Shan, L.; Xiao, G.; Li, A.; Zhou, S.; Wang, L.; Su, W.; Liu, Y.; Yang, L.; Song, X. Nonlinear forced vibration of the FGM piezoelectric microbeam with flexoelectric effect. *Alex. Eng. J.* **2025**, *110*, 386–399. [CrossRef]
39. Phuc, P.Q.; Van Dong, P.; Hai, N.T.; Zenkour, A.M.; Thien, L.G. The application of novel shear deformation theory and nonlocal elasticity theory to study the mechanical response of composite nanoplates. *Compos. Struct.* **2025**, *352*, 118646. [CrossRef]
40. Altenbach, H.; Meenen, J. Single Layer Modelling and Effective Stiffness Estimations of Laminated Plates. In *Modern Trends in Composite Laminates Mechanics. International Centre for Mechanical Sciences*; Altenbach, H., Becker, W., Eds.; Springer: Vienna, Austria, 2003; Volume 448, pp. 1–68. [CrossRef]
41. Sadeghian, M.; Palevicius, A.; Janusas, G. Nonlinear Thermal/Mechanical Buckling of Orthotropic Annular/Circular Nanoplate with the Nonlocal Strain Gradient Model. *Micromachines* **2023**, *14*, 1790.
42. Jomehzadeh, E.; Saidi, A.R. A study on large amplitude vibration of multilayered graphene sheets. *Comput. Mater. Sci.* **2011**, *50*, 1043–1051. [CrossRef]
43. Reddy, J.N. A simple higher-order theory for laminated composite plates. *J. Appl. Mech.* **1984**, *51*, 745–752. [CrossRef]
44. Reissner, E. On Tranverse Bending of Plates, Including the Effect of Transverse Shear Deformation. *Int. J. Solids Struct.* **1975**, *11*, 569–573. [CrossRef]
45. Touratier, M. An efficient standard plate theory. *Int. J. Eng. Sci.* **1991**, *29*, 901–916. [CrossRef]
46. Soldatos, K. A transverse shear deformation theory for homogeneous monoclinic plates. *Acta Mech.* **1992**, *94*, 195–220. [CrossRef]

47. Aydogdu, M. A new shear deformation theory for laminated composite plates. *Compos. Struct.* **2009**, *89*, 94–101. [CrossRef]
48. Mantari, J.; Oktem, A.; Soares, C.G. A new higher order shear deformation theory for sandwich and composite laminated plates. *Compos. Part B Eng.* **2012**, *43*, 1489–1499. [CrossRef]
49. Li, Q.; Wu, D.; Chen, X.; Liu, L.; Yu, Y.; Gao, W. Nonlinear vibration and dynamic buckling analyses of sandwich functionally graded porous plate with graphene platelet reinforcement resting on Winkler–Pasternak elastic foundation. *Int. J. Mech. Sci.* **2018**, *148*, 596–610. [CrossRef]
50. Reddy, J.N. *Energy Principles and Variational Methods in Applied Mechanics*, 3rd ed.; John Wiley & Sons, Inc.: Hoboken, NJ, USA, 2017.
51. Kerr, A.D.; Alexander, H. An application of the extended Kantorovich method to the stress analysis of a clamped rectangular plate. *Acta Mech.* **1968**, *6*, 180–196. [CrossRef]
52. Shu, C. *Differential Quadrature and Its Application in Engineering*; Springer Science & Business Media: Berlin/Heidelberg, Germany, 2000. [CrossRef]
53. Bellman, R.; Casti, J. Differential quadrature and long-term integration. *J. Math. Anal. Appl.* **1971**, *34*, 235–238. [CrossRef]
54. Altekin, M.; Yükseler, R.F. Large Deflection Analysis of Clamped Circular Plates. In Proceedings of the World Congress on Engineering (WCE 2011), London, UK, 6–8 July 2011.
55. Timoshenko, S.; Woinowsky-Krieger, S. *Theory of Plates and Shells*, 2nd ed.; McGraw-Hill New York: New York, NY, USA, 1959.
56. Szilard, R. *Theory and Analysis of Plates: Classical and Numerical Methods*; Prentice-Hall, Inc.: Englewood Cliffs, NJ, USA, 1974; p. 728.
57. Harik, I.E. Analytical Solution to Orthotropic Sector. *J. Eng. Mech.* **1984**, *110*, 554–568. [CrossRef]
58. Farajpour, A.; Mohammadi, M.; Shahidi, A.R.; Mahzoon, M. Axisymmetric buckling of the circular graphene sheets with the nonlocal continuum plate model. *Phys. E Low-Dimens. Syst. Nanostruct.* **2011**, *43*, 1820–1825. [CrossRef]